# A melanoma brain metastasis CTC signature and CTC:B cell clusters associate with secondary liver metastasis: a melanoma brain-liver metastasis axis

Tetiana Y. Bowley[1], Mireya C. Ortiz[1], Irina V. Lagutina[2], Mara P. Steinkamp[3], Bridget N. Fahy[4], Bernard Tawfik[5], Moises Harari-Turquie[5], and Dario Marchetti[1,3 *]

[1] Division of Molecular Medicine, Department of Internal Medicine, University of New Mexico Health Sciences Center, Albuquerque, NM

[2] Animal Models Shared Resource, The University of New Mexico Comprehensive Cancer Center, Albuquerque, NM

[3] Department of Pathology, University of New Mexico Health Sciences Center, Albuquerque, NM

[4] Division of Surgical Oncology and Palliative Medicine, University of New Mexico Comprehensive Cancer Center, Albuquerque, NM

[5] Division of Hematology and Oncology, Department of Internal Medicine, University of New Mexico Comprehensive Cancer Center, Albuquerque, NM

* Corresponding author: Dr. Dario Marchetti, Division of Molecular Medicine, Department of Internal Medicine, Department of Pathology, UNM Health Sciences Center, CRF, Room 305, 915 Camino de Salud, Albuquerque, NM
E-mail: dmarchetti@salud.unm.edu. Tel.: +(505) 272-7937.

**Running title**: The Melanoma CTC Brain-Liver Metastasis Axis

**Conflicts of Interest:** Authors declare no conflicts of interest.

Manuscript contains 8 Figures, 11 Supplementary Figures, and 4 Supplementary Tables.

## Abstract

Melanoma brain metastasis (MBM) is linked to dismal prognosis, low overall survival, and is detected in up to 80% of patients at autopsy. Circulating tumor cells (CTCs) are the smallest functional units of cancer and precursors of fatal metastasis. We previously employed an unbiased multilevel approach to discover a unique ribosomal protein large/small subunits (RPL/RPS) CTC gene signature associated with MBM. Here, we hypothesized that CTC-driven MBM secondary metastasis ("metastasis of metastasis" per clinical scenarios), has targeted organ specificity for liver. We injected parallel cohorts of immunodeficient and newly-developed humanized NBSGW (HuNBSGW) mice with cells from CTC-derived MBM to identify secondary metastatic patterns. We found the presence of a melanoma brain-liver metastasis axis in humanized NBSGW mice. Further, RNA-Seq analyses of tissues showed a significant upregulation of the RPL/RPS CTC gene signature linked to metastatic spread to liver. Additional RNA-Seq of CTCs from HuNBSGW blood revealed extensive CTC clustering with human B cells in these mice. CTC:B cell clusters were also upregulated in blood of primary melanoma patients, and maintained either in CTC-driven MBM or MBM CTC-derived cells promoting liver metastasis. CTC-generated tumor tissues were interrogated at single-cell gene and protein expression levels (10x Genomics Xenium and HALO spatial biology platforms, respectively). Collectively, our findings suggest that heterotypic CTC:B cell interactions can be critical at multiple stages of metastasis.

## Significance statement

This study provides important insights into the relevance of pro-metastatic CTC:B cell clusters in melanoma progression, extends the importance of the CTC RPL/RPS gene signature beyond primary metastasis/MBM driving targeted organ specificity for liver metastasis ("metastasis of metastasis"), and identifies new targets for clinical melanoma metastasis therapies.

## Introduction

Melanoma is the most aggressive skin cancer which associates with high metastatic burden, especially to brain (1-4). Melanoma brain metastasis (MBM) is detectable in

60% of advanced melanoma cases and up to 80% at time of autopsy (5-7). MBM represents the third most common origin of brain metastasis, surpassed only by lung and breast cancers (8,9), and is increasing in frequency. MBM patients have dismal survival rates and most will die from their disease in 4-6 months (10,11). Treatment of early-stage melanoma tumors includes surgical resection and radiation followed by adjuvant therapies, while metastatic melanoma is treated with systemic therapies. Although immunotherapies and targeted therapies have improved the prognosis of these patients, overall patient survival remains poor, and novel biomarkers/therapeutic approaches are desperately needed (10,12,13).

Cancer cells with unique properties intravasate into the bloodstream (Circulating Tumor Cells or CTCs), and initiate tumor formation at distant organs via a complex set of events (14-16). CTCs are the smallest functional units of cancer and “seeds” of fatal metastasis. CTCs encounter extensive microenvironmental, shear, and oxidative stresses in blood, and 99% die early prior to successful metastatic onset (17,18). However, subsets of CTCs can acquire a quiescent state and reside in bone marrow for years before their activation (18,19). CTCs can shed from the original primary lesion, thus promoting metastasis via their dissemination in blood, arrest, adhesion, and extravasation at distant organs, such as liver, lung, skin, and brain. Of note, CTCs can also intravasate from established metastases to further promote metastatic dissemination (“metastasis of metastasis”: the metastatic cascade)(14,20-22). Clinical metastasis therefore occurs at multiple sites sequentially and/or concurrently, and results in poor clinical outcomes and high mortality rates (23). Importantly, the number of CTCs in patients’ blood directly relates to cancer severity, metastasis, and overall patient survival (15,24). Furthermore, while CTC clusters (2 or more cells) comprise only 2-5% of all CTCs, their presence in blood indicates dramatically increased metastatic capabilities among cancer types, eg, 23-50 times higher than single CTCs which translates in poor patients’ survival (25-27).

CTC gene profiles are distinct from primary vs. metastatic tumors, and represent the gain of novel mutations or properties allowing for increased metastatic competence (19,28). Growing MBM onset and burden enables enhanced CTC shedding into

patients' bloodstream. Previously, we employed an unbiased, multipronged approach which resulted in the discovery of a unique 21-member RPL/RPS CTC gene signature associated with MBM and its progression in brain investigated spatially and temporally (1) [the term "RPL" refers to 60S or large ribosomal subunit, while "RPS" stands for 40S or small ribosomal subunit (29,30)]. Further, we funneled 4 RPL/RPS members of the melanoma CTC signature (RPL23, RPL35A, RPL6, and RPS18) out of 21 RPL/RPS genes to be keenly involved in metastatic progression: drug inhibitory studies, demonstrated that the dual targeting of cell translation/cell proliferation inversely affected CTC glycolytic metabolism in real-time, however it was critical to suppress CTC metastasis in immunodeficient mice (31). CTCs utilize aberrant ribogenesis to preferentially translate oncogenic RNA transcripts to initiate metastatic dissemination and progression: enhanced ribosomal RPL15 synthesis was reported to be directly linked to breast cancer metastasis (32,33). Moreover, the trend of enhanced tumor-specific total mRNA synthesis (TmS) has been observed in 6,580 patients across 15 different cancer types and correlates with poor clinical prognosis (34).

Noteworthy, multiple studies have identified heterotypic clustering of CTCs with normal cells, including neutrophils, polymorphonuclear-myeloid derived suppressor cells (PMN-MDSCs), CD3 cells, CD4 cells, and platelets in metastatic patients (25-27,35). For example, the presence of as little as one CTC-neutrophil cluster in patient's blood was linked to lower survival rates and worse clinical outcomes if compared to patients with no heterotypic CTC clusters (35).

Here, we provide first-time evidence that CTC-driven primary MBM has a liver-targeted organ specificity to generate extensive secondary metastasis to liver, thus discovering the presence of a CTC brain-liver metastasis axis. Second, we report the presence of CTC:B cell clusters, and detection of high number of these clusters in blood of primary melanoma patients with no clinical evidence of metastasis. Conversely, CTC evaluation of metastatic melanoma patient blood revealed a 15/20-fold decrease in CTC:B cell clusters. These findings implicate their relevance early in the metastatic cascade, and substantiate notions that melanoma B cell phenotypes interacting with CTCs can be pro-metastatic and predict disease severity and clinical outcomes (36,37). Third, by

employing a unique humanized NBSGW (huNBSGW) mouse model which possess high peripheral blood B cell numbers (38,39), we provide evidence for CTC:B cell implications in melanoma progression, eg, from primary MBM to secondary metastatic disease, closely reflecting the clinical scenario ("metastasis of metastasis"). To this end, first-generation CTC xenografts (CDXs) were generated by intracardiac injection of MBM-competent CTCs while second-generation CDX mice were developed by engrafting blood or MBM cells from the first-generation, revealing the presence of CTC:B cell clusters in both generations. Lastly, we report that these pivotal interactions are present either at the level of blood, or brain and liver tissues by employing the cutting-edge single-cell 10x Genomics Xenium™ (gene expression) and Indica HALO™ (protein expression) spatial biology platforms. The extensive liver metastasis observed in the second-generation NBSGW mice injected with MBM-derived cells had highly elevated expression of the RPL/RPS gene CTC signature of MBM, fostering relevance of this signature in the brain-liver axis of melanoma. Altogether, these findings provide a conduit for therapeutic targeting CTC:B cell clusters which could inhibit metastasis and thus render more patients curable.

## Materials and Methods

### Patients' blood collection

Blood samples from patients with either primary melanoma or metastatic melanoma were gathered according to the protocols approved by the Institutional Review Board at UNM Health Sciences Center (UNM-HSC) in Albuquerque, New Mexico. Primary melanoma was defined as tumor confined to the original site of disease that was resected with curative intent. Blood was taken prior to definitive surgical resection of the primary tumor and nodal staging. Conversely, metastatic melanoma refers to blood taken from patients with tumor spreading to brain, liver, lung, and other skin locations outside the original site. Clinical information about each patient is provided. Patients signed informed written consent before the scheduled sample collection. Using aseptic technique, the patient's peripheral blood (15-25 mL) was drawn from the middle of the vein puncture and into an EDTA tube as part of their medical appointment. Samples were transported to the laboratory where isolation and interrogation of CTCs took place.

These samples were either processed immediately or preserved in CellSave™ (Menarini Silicon Biosystems, Inc., Huntingdon Valley, PA), or Streck Cell-Free DNA BCT tubes (Streck, La Vista, NE).

**CTCs/CTC clusters isolation**

Blood from mice (100-300 µL) was drawn retro-orbitally using an EDTA-coated glass pipette and transferred into Greiner MiniCollect collection tubes (Greiner Bio-One, Cat# K3E K3EDTA, Monroe, NC). Blood was then loaded onto the FDA-approved CTC Parsortix™ microfluidic chip (pore size 6.5 µm) within an hour or two of necropsy. The Parsortix PR1 Platform (Angle Europe Ltd., Surrey, UK) with 6.5 M cartridge (Angle, PLC) was used to capture single CTCs and CTC clusters through filtration and microfluidic methods. CTCs were identified as cells stained for human Mel-A (labeled with Alexa Fluor 594, Santa Cruz Biotechnology, Cat#sc-20032, Dallas, TX), human CD45 (FITC-tagged, BioLegend, Cat# 103108, San Diego, CA), and DAPI (Thermo Fisher, Cat# D3571, Waltham, MA). CD19 antibody (Monoclonal Antibody (H1B19), Thermo Fisher, eBioscience, Cat# 14-0199-82, Waltham, MA) was used to stain B cells. CTCs were observed and counted using a Zeiss LSM800 microscope (10x and 40x magnification) and analyzed with ZEN Blue 2.1 software (Carl Zeiss Microscopy, Oberkochen, Germany).

**Cell culture**

Highly brain-metastatic melanoma CTC-derived clonal cells (70W-SM3; generated in Dr. Marchetti's laboratory) were grown as previously described (1). The luciferase-tagged CTC clone cells (70W-SM3-Luc2) were prepared as previously described (40). Briefly, CTC-derived clonal cells were cultured with DMEM/F12 (Thermo Fisher, Cat#11320081), supplemented with 10% fetal bovine serum (FBS) (Gibco, Cat#A4766801, Billings, MT) and 1x GlutaMAX (Gibco, Cat#35050061). The cells were maintained at 37°C in a humidified chamber with 5% $CO_2$. Cells were passaged using Accutase (STEMCell Technologies, Cat#07922) or 0.05% trypsin-EDTA (Gibco, Cat# 25300054) before reaching their maximum confluency.

**Humanized NBSGW mouse model**

Humanized NBSGW (HuNBSGW) mice were engrafted by the UNM-CCC Animal Models Shared Resource. Frozen human CD34+ cord blood cells from mixed donors (CD34+ CBC) were purchased from Human Cells Biosciences (Cat# CBCD34-mix-C1M, Milpitas, CA). One million cells were thawed according to the manufacturer recommendations. The cells were then washed twice with Stemline® II Hematopoietic Stem Cell Expansion Medium (S0192, Sigma-Aldrich). The donor cell pellet was resuspending in 1 mL of StemSpan™ SFEM II medium (09605, STEMCell Technologies Inc.) supplemented with 0.1 µg/ml Human Recombinant SCF (78062.1, STEMCell Technologies Inc.) prior to cell counting. Cells were then seeded in a 24-well plate and allowed to recover overnight (12 hrs) in a cell culture incubator (5% CO2 at 37C). Afterwards, CD34+ CBC were resuspended in PBS and injected into the livers of 1–3-day old NBSGW mice as described (41). Humanization rate (% human CD45+ cells in peripheral blood) was assessed at 12 weeks post-injection by flow cytometry with an antibody panel including a human-specific (clone HI30, BD Bioscience) and a mouse-specific (clone 30-F11, BD Bioscience) anti-CD45 antibody as described previously (38).

**CTC-derived xenografts (CDXs)**

Mouse studies were approved by the UNM Institutional Animal Care and Use Committee (IACUC). CDXs were generated using 6-12 weeks old NBSGW (NOD.Cg-KitW-41J Tyr + Prkdcscid Il2rgtm1Wjl/ThomJ) mice. Twenty four huNBSGW and twenty four NBSGW mice were injected retro-orbitally with 50 µL (4 mg/mL) of low-molecular weight heparin (NDC, Cat# 63323-533-01) prior to intracardiac injection to avoid thromboembolism. Mice were anesthetized with isoflurane (2.5%, 1 L/min O2 flow) and 5.0 x $10^5$ CTC-derived clonal cells (passage 18) were injected into the left ventricle of the heart with a sterile 0.5-mL U-100 insulin syringe with a 29Gx1/2” needle (Beckton Dickinson, Cat# 58324702). Blood backflow confirmed successful intracardiac needle placement. Longitudinal bioluminescent imaging of tumor burden using the IVIS Spectrum *in vivo* imaging system (PerkinElmer, Waltham, MA) was performed weekly to monitor tumor development in mice. After 6 weeks, 5 MBM male and 5 MBM female mice from both cohorts (humanized and non-humanized) were euthanized and

necropsied. Samples from huNBSGW with MBM were re-injected into a second generation of HuNBSGW hosts, while samples from non-HuNBSGW with MBM were re-injected into non-huNBSGW hosts. Blood was collected and re-injected retro-orbitally (350 µL) into second generation mice ("blood-derived" mice), both humanized and non-humanized NBSGW cohorts. Brain tumors were isolated based on their black-to-brown pigment, dissociated using Accumax (STEMCell Technologies, Cat#07921), and engrafted as a single-cell suspension of 5.0 x $10^5$ cells in PBS by intracardiac injection into the second generation of mice ("brain-derived" mice). A schematic recapitulating the experimental plan is shown in Suppl. Figure 3). All mice were monitored daily for signs of lethargy and distress, such as sudden weight loss, unkempt fur, difficulty with breathing, seizures, and neurological problems. At a humane endpoint, mouse blood was collected into an EDTA-containing MiniCollect tube (Greiner Bio-One, Cat# K3E K3EDTA). CTCs were isolated using the FDA-approved CTC Parsortix™ platform, and RNA was extracted for further RNA-seq. Brain, liver, lungs, and spleen were fixed (10% formalin) for Xenium™ (10x Genomics) and HALO™ (Indica Lab.) analyses.

**RNA-Seq**

Following Parsortix™ CTC capture (Angle, LLC, Plymouth Meeting, PA, USA), RNA was isolated from enriched and flow-through fractions (10-20 x $10^3$ cells). The enriched fraction was comprised of human CTCs, while the flow-through fraction contained immune cells. The mRNA was extracted using the RNeasy Micro Kit (Qiagen, Cat # 74004, Hilden, Germany) following the manufacture's protocol. The RNA was analyzed, cDNA was synthesized, and library preparation were utilized by the microarray platform SMARTer Universal Low Input RNA kit for RNA sequencing (Clontech, Cat#634946, San Jose, CA). Fragmented RNA underwent processing using the Ion Plus Fragment Library kit (Thermo Fisher, Cat#4471252, Waltham, MA). The samples were sent to be sequenced on the Ion proton S5/Xl platform (Thermo Fisher, Waltham, MA) at the Analytical and Translational Genomics (ATG) Shared Resource Core located at the University of New Mexico Comprehensive Cancer Center (UNM-CCC).

**Bioinformatics and biostatistical analyses**

Tmap (v5.10.11) was used to align RNA-Seq analyses to a BED file format with nonoverlapping exon regions. Exons were quantified using HTSeq (v0.11.1)(42). Counts across exons were averaged to generate the gene-level counts. EdgeR was used to normalize the size of the library and to perform differential analysis (43,44). Heatmap3 was utilized to generate heatmaps and cluster analyses. Enrichment of pathways were conducted through the Reactome database, as previously described (45).

### 10x Genomics Xenium™ analyses

Tissue sections were processed using the manufacturer's guidelines for Xenium (10x Genomics; www.10xgenomics.com). Both the standard pre-designed human multi-tissue/cancer panel (10x Genomics, product number 1000626), as well as a custom designed panel [30 customized genes, including all 21 members of the RPL/RPS CTC signature (B)], were employed to generate the 10x Xenium results. Decoding of optical transcript signals and cell segmentation were computed using the on-board software (v2.0.0.10) resulting in transcript assignment to cells. The resulting count and image files were further analyzed with Seurat (v. 5.0.1) to visualize clustering and custom transcript location (46,47).

### Indica HALO™ analyses

Following necropsy, liver and brain tissues from 1st- and 2nd-generation NSBGW and HuNBSGW mice were fixed immediately in 10% formalin. Fixed tissues were paraffin embedded and sectioned and immunohistochemistry to detect infiltrating immune cells was performed on the Ventana Discovery Ultra Platform using immunoperoxidase labeling by the UNM Human Tissue Repository (HTR). The slides were labelled with hematoxylin as a nuclear counter stain for cell identification and Roche DISCOVERY Purple (RUO) chromogen staining to identify MelanA. All tissue slides were scanned using the Leica Aperio AT2 digital scanner at 20x magnification. Quantitative analysis of MelanA positive cells and immune cell infiltration was performed using the HALO analysis and annotation software package (Indica Labs, Albuquerque, NM). Mel-A was consistently expressed in MBM/liver xenograft tissues (Figure 8) (19). Notably, we consistently detected high melanin content in MBM and other metastatic lesions, which

suggests a direct correlation between Mel-A expression in patients and aggressive disease. Further, the HALO system parameter for positivity intensity was set to the optical density threshold of 0.02. The system's Figure Maker feature was used to generate the magnification series of images with and without HALO markup.

## Data Availability

The data generated in this study are publicly available in Gene Expression Omnibus (GEO) at GSE280739 and GSE280741, per NIH guidelines and schedule.

## Results

### Establishment of the humanized MBM CDX model

Interrogating the importance of the immune system in melanoma progression and metastatic onset enabled us to generate the first humanized MBM CTC-xenograft (CDX) model. Previously, we reported the development of the first immunodeficient CDX melanoma model (1). We used non-irradiated humanized NBSGW (HuNBSGW) animals to generate a more clinically relevant model (38). HuNBSGW mice (12 males, 12 females) were injected with CTC-derived Luc-tagged clonal cells, as previously reported (1,31). The CTC clonal cell line was tagged with the Luc2 protein in order to monitor metastatic spread and change in tumor burden over time by bioluminescence imaging and to optimize collection time points for IVIS imaging**.** The CTC-derived clone is highly aggressive with MBM detected as early as 24 hrs following intracardiac injection (1). It has been reported that expression of foreign proteins such as luciferase may impact immune response. However, this effect is not only highly dependent on the cell line (48), but also on the mouse model used. Parallel experiments with intracardiac injections of the Luc2 CTC-derived clonal line (70W-SM3 cells) in immunocompromised (NSG or NBSGW), and HuNBSGW mice showed that the time from injection to fully developed metastatic melanoma, which required humane euthanasia, was the same (no statistical difference), suggesting that immunogenicity of Luc2 under our experimental conditions was negligible. Successful engraftment of immune system cells was confirmed by flow cytometry and by the presence of tumor-infiltrating lymphocytes (TILs) and tumor associated macrophages (TAMs) in brain/liver metastases by tissue

immunostaining for CD3, CD4, CD8, CD68, human mitochondrial marker, and CD19 immune biomarkers (Fig. S1A)(38). The percentage of infiltrating human immune cells (number of positive stained cells/total number of cells in the section) was computed using HALO software (N=3; Fig. S1B). Tissues from mice with similar humanization levels were used to perform HALO analyses. Due to difficulty of humanizing the male mice, several huNBSGW mice had lower than 20% humanization rates; however, even lower humanization mice had infiltrating immune cells in metastases and showed difference in metastatic patterns, compared to non-humanized mice. No clinical symptoms of graft-versus-host disease were observed in any of the HuNBSGW animals. Importantly, the level of humanization of $1^{st}$- and $2^{nd}$-generation mice was adequate to perform studies described (Supplementary Table 1).

A cohort of 24 immunodeficient NBSGW mice was engrafted with CTC-derived clonal cells in parallel. Metastasis occurrence and progression were monitored by weekly IVIS imaging. A percentage of humanized and immunodeficient mice presented with MBM (Figs. 1A/1B). Quantification of MBM tumor burden (total flux) by IVIS imaging confirmed time-dependent MBM progression in both models (Fig. S2). Notably, animal necropsies had extensive MBM in huNBSGW and NBSGW mice (Fig. 1C/1D). Additionally, melanoma cells disseminated to the liver (Fig. 1E), lungs, intestine, bone marrow, and spleen, recapitulating target organ metastatic specificity of clinical melanoma (49). This set of animals was designated “first generation” mice.

At the end of the study, MBM tumors from 10 huNBSGW were dissociated and engrafted by intracardiac injection as a single-cell suspension into “second-generation” of huNBSGW mice to interrogate site preference of MBM cancer cells. Likewise, MBM from non-huNBSGW mice were engrafted into second-generation non-huNBSGW. In parallel, another cohort of mice was injected with blood from the first-generation mice to compare metastatic target organs of blood-residing CTCs with MBM tumor cells. Humanization in the second-generation mice was confirmed prior to engraftment of blood/MBM cells (Supplementary Table 2). A flowchart depicting the detailed outline of experimental procedures is presented in Fig. S3.

**MBM-competent CTCs promote extensive secondary liver metastasis**

IVIS quantification of MBM signal was performed (Fig. S4). The second-generation mice were necropsied eight weeks post-injection of brain cells or blood. Importantly, major differences were detected in metastatic patterns in the presence or absence of human immune cells in these mice. First, second-generation HuNBSGW mice engrafted with MBM developed extensive liver mets (Fig. 2A) which were significantly larger in size and numbers than second-generation NBSGW (Fig. 2B), or first-generation HuNBSGW liver tumors. Second, blood-injected animals, regardless of immune competency, did not develop any liver mets (Fig. 2C). Interestingly, blood-injected CDXs developed MBM earlier than brain (MBM-derived cells)-injected CDXs. Third, there were differences in MBM occurrence in the presence of human immune cells: a higher number of HuNBSGW mice developed MBM than immunodeficient animals (40% versus 20% MBM mice; Fig. 2A/2B, bottom panel). The comparison of all metastatic sites between the two groups is presented in Table S3.

Previously, we employed an unbiased and multipronged approach to identify a specific 21-member RPL/RPS melanoma CTC signature associated with MBM (1). To investigate it further, we performed RNA-Seq on brain- and liver-dissociated cells isolated from second-generation HuNBSGW mice, injected with brain tumor cells. Transcriptional profiling of brain- and liver-derived tumor cells showed distinct clustering patterns in brain tumor versus liver tumor cells (Fig. 3A, right panel). Intriguingly, HuNBSGW liver cells had a five-fold increase in the RPL/RPS gene expression, compared to brain cells from the same mice (Fig. 3A, left panel). This observation suggests that brain-derived melanoma cells target liver where they establish a tumor-promoting niche and develop extensive liver metastasis. Thus, there may be a brain-liver axis in melanoma. The Reactome$^{TM}$ pathway software analyzed differential gene expression between samples and produced a list of statistically significant pathways (Fig. 3B). Importantly, the majority of differential pathways were CTC RPL/RPS gene pathways (highlighted in yellow) (1). These translational pathways play a critical role in cancer progression (50).

**B-cell clustering with MBM-competent CTCs**

To quantify CTC numbers and identify CTC traveling partners, we captured and analyzed CTCs from immunodeficient and HuNBSGW groups using the CTC Parsortix microfluidic platform. In each group (Fig. S3 flowchart), an equal volume of pooled blood was analyzed via Parsortix to capture and isolate human CTCs based on their size and deformability. Individual CTCs and CTC clusters were immunostained for human CD45-FITC, human MelanA Alexa 594, and DAPI nuclear marker. Mel-A+/DAPI+/CD45- cells were defined as melanoma CTCs, imaged via confocal microscopy and enumerated (Figs. 4A and 4B). Healthy donor blood was used as a negative control to confirm the presence of CD45+ cells and the absence of melanoma CTCs (Fig. 4C). A considerable increase (up to a ~20-fold difference between HuNBSGW and NBSGW) of single CTCs and CTC clusters was detected in the blood of HuNBSGW mice (Fig. 4C, bottom panel). The presence of CTC clusters indicates strong metastatic competence and cancer severity (26,27). Importantly, both homotypic and heterotypic CTC clusters were detected in the blood of HuNBSGW mice (Fig. 4B). CD45+ staining was used to identify CTC clustering with white blood cells; interestingly, CTC traveling partners were CD45- in CTC clusters.

For further interrogation of heterotypic CTC clusters, blood from three MBM HuNBSGW mice was collected via retro-orbital draw. Parsortix was used to capture and harvest single CTCs and CTC clusters for single-cell RNA-Seq analysis. Unsupervised hierarchical clustering between CTCs and uninjected CTC clonal cells showed obvious distinctions in clustering patterns between samples (Fig. 5A, top panel). Analyses of differential gene expression via the Reactome database generated a list of molecular pathways, including immune pathways (Fig. 5A, bottom panel). Importantly, the most statistically significant pathway was a B cell-related pathway “CD22 mediated BCR regulation” that was upregulated in CTC clusters from HuNBSGW blood. A list of the 20 most statistically significant pathways included another B cell-related pathway, additive to previously reported interactions of CTCs with PMN-MDSCs, platelets, neutrophils CD3, and CD4 cells in CTC clusters (26,27,35). Since uninjected CTC-derived clonal cells did not contain any immune cells, the presence of B cell pathways in this analysis showed B cell clustering specificity with MBM-competent CTCs. To confirm that findings are not model-dependent, we performed blood RNA-Seq comparisons between

HuNBSGW and immunodeficient NSG mice, both injected with the same CTC-derived clonal line, as previously described (1). Transcriptional profiling showed discordance between CTC/CTC clusters according to presence or absence of human immune cells (Fig. 5B, top panel). Notably, Reactome-generated list of statistically significant pathways contained B-cell related pathways (Fig. 5B, bottom panel). Further interrogation of CTC:B cell interactions prompted us to expand our analysis to other tissues, such as brain (Fig. 5C). Brain tumors from 2$^{nd}$-generation NBSGW and HuNBSGW mice were dissociated and interrogated via RNA-Seq. Hierarchical clustering between these samples showed distinct discordance between the samples (Fig. 5C, top panel). Reactome analyses of differential gene expression produced statistically significant pathways, including two B-cell related pathways (Fig. 5C, bottom panel). Few B cells were identified in HuNBSGW first-generation brain tumors, and first- and second-generation liver tumors (Fig. S1A). Altogether, HuNBSGW studies showed important clustering between B cells and melanoma CTCs, which was independent of mouse models and tissues.

To confirm CTC:B cell clustering in clinical settings, melanoma patient blood was immunostained via Parsortix for human CD19-488, human MelA Alexa 594, and DAPI (Fig. 6A, Fig. 6B, Fig. 6C, left panels). CTC:B cell interactions were visualized and quantified using high-definition confocal microscopy. Blood was provided from primary and metastatic melanoma patients. Primary patients did not have any clinical-diagnosed metastasis and did not receive any treatment or immunotherapy, other than surgical removal of primary tumor in conjunction with nodal staging with sentinel lymph node biopsy (patients' clinical parameters are shown in Supplementary Table 4). Of relevance, the number of CTC:B cell clusters in primary patients was 15-20-fold higher than in metastatic patients (Fig. 6A, Fig. 6B, Fig. 6, right panel). These observations suggest that CTC:B cell clusters may be critical in the early stages of CTC dissemination towards metastatic onset.

**B-cell crosstalks with CTC-derived tumor cells by 10x Genomics Xenium**

To explore interactions between CTC-derived cells and B cells at tissues level, we employed single-cell spatial transcriptomics (10x Xenium platform). HuNBSGW A2.1

mice were used to match HLA of the CTC-derived clone with the humanized mouse model. Eight HuNBSGW A2.1 mice intracardiacally injected with the CTC-derived clonal cells, followed by 3D IVIS tomography confirming metastasis to brain, liver, and intestine (Fig. S5A). Representative brain, liver, and intestine mouse tumors were fixed, paraffin-embedded, sectioned and used for H&E staining (Fig. S5B), spatial transcriptomics via the single-cell Xenium platform (Figs. 7, Fig. S6, top panel), and further protein immunostaining/HALO analyses (Fig. 8, Fig. S7). Dim Plot analysis of tumor tissues visualized plots of cells in a reduced-dimensional space on a 2D scatter plot (Fig. 7A), while bar plot analyses determined the percentage of all samples in clusters (Fig. S8). Heatmaps of HuNBSGW vs NBSGW tissues indicated distinct differences of gene expression in the presence or absence of human immune cells (Fig. S9, Fig. S10, Fig. S11).

The custom-designed 10x Xenium gene panel contained human 30 genes, including pathologically-established B cell receptor (BCR) and S100A1 melanoma markers, and RPL23, and RPL35A as most representative members of the melanoma CTC signature. We have previously reported that RPL23 and RPL35A are two RPL/RPS members out of 21 CTC RPL/RPS gene signature that are downregulated in response to translation and proliferation inhibition (31). These two biomarkers were used to compare RPL/RPS transcript counts in melanoma vs surrounding cells. Spatial transcriptomics confirmed clustering of CTC-derived melanoma cells with B cells in humanized MBM and liver (Fig. 7B, top left panel, Fig. 7B, top right panel), liver (Fig. 7, top right panel), and intestine (Fig. S6). The number and percentage of S100A1 and BCR transcripts in tumor tissues are shown (Fig. 7, bottom panel; Fig. S6, bottom panel). RPL/RPS gene transcript expression was significantly higher in CTC-derived melanoma than human immune cells (Fig. 7B, and Fig. S6).

**HALO analyses**

To perform an unbiased tissue quantitation, we employed the HALO system of the whole-slide imaging analyses of HuNBSGW tissues brain with MBM (Fig. 8A, Fig. 8B, top panel, and Fig. S7). Tissues were stained with MelA and CD19 to visualize human melanoma and B cells, respectively. The whole tissue is shown in the left image of the

panels, with close-up views to follow. Quantification of the number of MelA and CD19+ B cells was performed using the HALO software (Fig. 8B, bottom panel). Importantly, areas with a high percentage of tumor cells showed intravasation of B cells in those areas. Physical interactions between B cells and tumor cells are visible in the close-up images (right panels). Collectively, HALO analyses confirmed not only presence of human B cells in metastatic lesions but also their significant interactions with CTC-derived melanoma cells.

## Discussion

CTCs intravasate into the blood stream from primary and metastatic tumors to establish either primary or secondary metastasis ("metastasis of metastasis") (14,51). The development of organ-specific metastasis is not random, but rather a complex, continuous and highly selective process with target organ metastatic specificity unique to each cancer type (14,52,53). Melanoma metastasis occurs at multiple sites, including brain, liver, lung, spleen, pancreas, lymph nodes, and bone (54). In addition, metastasis consist of heterogenous cell populations which introduce many challenges for selecting a successful treatment. Patients diagnosed with MBM often present with liver metastasis and this associates with poor clinical prognosis (55). Here, by employing the newly developed NBSGW mouse model and injections of a melanoma CTC-derived clone in sequential generations of mice (Fig. S3 flowchart), we provide first-time evidence that: 1) CTC-driven primary MBM has target organ specificity to generate extensive secondary metastasis, notably to liver, supporting the presence of a CTC brain-liver metastasis axis; 2) the detection and upregulation of CTC:B cell clusters closely relate to melanoma progression from primary to secondary metastatic disease; 3) commonality, association, and upregulation of the RPL/RPS MBM CTC gene signature were not only significantly maintained but also amplified in CTC-MBM secondary liver metastasis.

Only original brain tumor (MBM)-resident cells gave rise to liver metastasis in the second-generation of HuNBSGW mice since second-generation animals injected with blood from the first-generation blood-injected animals did not develop any metastasis to the liver. For blood-injected animals, only MBM onset was observed (Fig. 2C). This

dichotomy can be ascribed to distinct properties these cells have before or after intravasation in blood. However, the metastatic pattern for liver metastasis was detected, which recapitulates the clinical characteristics of melanoma patients, notably ones diagnosed with MBM (55). Multiple events must occur for cells to leave the brain and metastasize to liver, eg, blood intravasation, survival in the circulation, arrest to the target organ, adhesion, invasion, micro-metastatic onset. All these steps involve complex mechanistic events, which are still unclearfor the most part and are the subject of active investigations. Our scope was to delineate the biological events of secondary metastasis by performing “CTC-centric” experiments which centered on the CTC RPL/RPS gene signature of melanoma brain metastasis (MBM), and the validity of this CTC signature not only for MBM onset but beyond. – We addressed the hypothesis that MBM CTCs possessing this signature drive extracranial secondary metastasis (“metastasis of metastasis”), notably to the liver as we have herein demonstrated. While we cannot prove the direct movement of CTCs from MBM to the liver, we can state that cells originating from CTC-driven MBM (1$^{st}$ generation mice) expressing the RPL/RPS gene signature have a predilection to colonize the liver vs other organs. Cells originating from CTC-MBM (1$^{st}$ generation of mice) possessing the RPL/RPS gene signature have a predilection to colonize the liver versus other organs, in parallel to augmented expression of the signature. Furthermore, using the sensitive Luc2 reporter, we were able to detect metastases in the brain of these animals 24 hours following injection. Conversely, liver mets were detected at much later times (10-15 days) in the disease progression. We consider these findings relevant for their clinical implication, eg, linking MBM with liver metastasis within the clinical metastatic cascade seen in patients. We consider these findings highly relevant for their clinical implication, eg, linking MBM with liver metastasis within the clinical metastatic cascade seen in patients. The CTC-driven brain-liver metastasis axis has been postulated in other cancers, eg, by the injection of Lin-/CTC populations isolated from triple-negative breast cancers (TNBC) diagnosed with brain metastasis in sequential generations of CDXs (immunodeficient NSG mice), however with neither direct confirmation, or in the presence of functional human immune system cells (56).

The cell populations of the brain tumor microenvironment are primarily composed of neurons, astrocytes, oligodendrocytes, and microglia, while the liver microenvironment is dominated by hepatocytes (parenchymal cells) alongside a large population of non-parenchymal cells including Kupffer cells (resident macrophages), hepatic sinusoidal endothelial cells (LSECs), and various other immune cell subsets, making the liver significantly more immune cell-rich compared to the brain. Furthermore, the brain has a highly selective blood-brain barrier restricting the entry of many molecules and immune cells, making the brain microenvironment relatively immune-privileged compared to the liver. Accordingly, liver TME contains a much broader range of immune cells including various T cell subsets, dendritic cells, natural killer cells, and neutrophils, depending on the physiological/pathological state.

Noteworthy, RNA-Seq demonstrated a statistically significant five-fold increase in the RPL/RPS CTC gene signature in MBM-derived liver metastasis relatable to a brain-liver metastasis axis (Fig. 3). We surmise that extensive liver metastases had increased RPL/RPS gene expression to alter ribosome structure, composition and function, eg, “onco-ribosomes” promoting augmented protein translation, oncogenic signaling pathways, and/or other cellular properties required for the multiple metastatic steps (57). Furthermore, increased ribosomal synthesis is also linked to metabolic plasticity which is pivotal for tumor cell survival and tolerance of oxidative/nitrosative stresses (50,55). To this end, we have previously reported that dual in vivo targeting of both CTC translation and proliferation is critical to rewire metabolic plasticity of CTCs (31). The discrimination of onco-ribosomes structural composition, protein:protein interactions, and their function (active vs dormant types) are currently underway, and involves the use of cryogenic electron microscopy (Cryo-EM) (58).

Another important finding of this study is that MBM-derived liver metastasis was detected only in humanized mice, and associated with CTC:B cell clustering. We employed a non-irradiated HuNBSGW mouse model that accurately recapitulates the genetic heterogeneity of human immune cell system populations, and recruits immune cells to tumor sites (38). Our data show that humanized immune cells clearly had an impact on melanoma progression in this in vivo model which more closely reflect the

complexity of the blood/tumor microenvironment found in patients. By performing unbiased analyses of peripheral blood from primary (blood collected adjacent to the primary lesion) and metastatic melanoma patients using the FDA-approved CTC Parsortix$^{TM}$ platform, we detected high numbers of CTC:B cell clusters explicitly in the former with a 15/20-fold decrease in the latter (Fig. 6, right panel). In addition, while parallel cohorts of first- and second-generation NBSGW mice were treated exactly in the same conditions as HuNBSGW mice, not only a lower percentage of NBSGW mice developed liver mets vs humanized NBSGW mice (20% vs 40%), but also at a significantly decreased size, eg, macro- vs micro-mets (latter defined as at least 0.2mm but no larger than 0.2mm or 200 cells) (Fig. 2B). With engraftment of luc-tagged CTC-derived clonal cells in HuNBSGW mice, human tumor-associated macrophages and tumor-infiltrating lymphocytes were detected in brain and liver tumors (Fig. S1). Future studies will determine the mechanistic underpinnings of how B cells support the progression of MBM CTCs to promote liver metastasis.

The presence of immune cells in the HuNBSGW mouse allowed us to explore CTC clusters in these mice. CTC clusters comprise only 2-5% of all CTCs, however the degree of the disease severity, either clinically or preclinically, is directly proportional to their number (24,25,27). Of these, heterotypic CTC clusters include normal immune cells, such as PMN-MDSCs, neutrophils, CD3 cells, CD4 cells, and platelets (25-27,35). To our knowledge, this study reports first-time evidence of heterotypic CTC:B cell clusters associated with clinical or experimental melanoma metastasis (Figs. 5 and 6). B cells can contribute to innate and adaptive immune response, underscoring the relevance of understanding how B cells in and their various subsets function in metastasis (36,59). For example, a recent study has demonstrated that B cell infiltration in the tumor microenvironment is linked to poor clinical outcomes and cancer immunotherapy resistance (60). Pro-metastatic roles of B cells have been reported in other cancer types, such as ovarian and bladder cancers (61-64). Tumor-infiltrating B cells induce the secretion of the pro-angiogenic marker lymphotoxin, which activates NF-κB signaling and promotes tumor progression (65-67). Additionally, B cells enable tumor development through the production of tumor growth factors, such as TGFβ, IL-10, and IL-35 (67). We extended these findings by detecting and analyzing interactions

between melanoma cells/CTCs with B cells either in blood (CTC clusters), or CTC-derived primary/secondary metastasis by single-cell gene or protein expression (10x Genomics Xenium and HALO spatial biology systems, respectively) (Fig. 7, Fig. 8). The crosstalk between the immune microenvironment and cancer cells is highly complex, but our findings suggest that the interrogation of CTC:B cell cluster functionalities may serve as a prognostic factor in the systemic evaluation of cancer progression and determination of the appropriate treatment approach.

This study has some limitations. First, we analyzed a limited number of melanoma primary and metastatic patients. Therefore, we cannot conclude that the observed heterotypic CTC:B cell clusters will be detected in blood of all melanoma patients. Similarly, the use of a single CTC-derived clone may not faithfully recapitulate the extensive CTCs/tumor heterogeneity detected in melanoma patients. Second, we did not directly associate presence of increased RPL/RPS gene expression with presence of CTC:B cell clusters. Mechanistic studies to affect this signature as result of CTC:B cell clustering are warranted. Third, we did not characterize specific B-cell subclusters, B cell signaling, and/or Breg functionalities which may modulate tumor progression. The identification of specific B-cell subclusters can be relevant to assess disease severity and to prescribe more suitable treatment for an individual patient. Lastly, while we performed experiments where a primary tumor was established with 2nd generation cells by subcutaneous injection in HuNBSGW and NBSGW mice, mice had to be euthanized due to the size of primary SQ tumors (humane end point of experiment) before they developed any metastases. Very few single CTCs were detected in blood of either HuNBSGW or NBSGW mice at time of necropsy, preventing further analyses. Additional investigations are warranted to address these limitations. Regardless, this study reports first-time evidence of a brain-liver metastasis axis which associates with presence of B cells acting as traveling partners of melanoma CTCs, and foster additional investigations of their roles in primary and secondary metastasis. There are consistently fewer B cell frequencies in distant sites vs the primary tumor across metastatic sites (36,68). However, the precise mechanisms that underpin B cell clustering with CTCs and/or the reduced B cell surveillance in the metastatic sites are critical but yet to be fully evaluated. A potential interpretation of our findings is that CTC-

derived cells:B cell clusters intravasate from MBM once generated, which makes the high percentage of B cells in HuNBSGW brain relative to livers (Fig. 7, bottom panel) extremely relevant in secondary metastatic disease. Their definition could provide an important conduit for translation in the clinic and the development of effective therapeutic agents to improve melanoma patient care.

**Acknowledgements**

This study was supported by the NIH grant 1R01 CA216991, the UNM-CCC Translational Initiative (TSI), and the Oxnard Foundation (to DM). Further, research was partially supported by UNM Comprehensive Cancer Center Support Grant NCI P30CA118100 that funds the UNM-CCC Shared Resources including the Analytical and Translational Genomics (ATG) Shared Resource, which receives additional support from the State of New Mexico, the Animal Models Shared Resource (AMSR), and the UNM Human Tissue Repository (HTR) Shared Resource. The University of Colorado Anschutz Medical Campus Genomics Shared Resource is funded by the Cancer Center Support Grant P30CA046934. We want to extend our gratitude to all melanoma patients who donated their blood to this study. We thank Fred Schultz and Cathleen Martinez of UNM HTR, and Kathryn Brayer and Kel Cook of the ATG for performing HALO/Xenium and RNA-seq analyses, and Lillian Fitzpatrick of AMSR for her technical support for animal studies. We are grateful to Olufunmilola Oyebamiji of ATG for conducting bioinformatics analysis and translational profiling. We want to acknowledge UNM-CCC clinical coordinators Leslie Garcia and Valerie Parks who approached melanoma patients for a written consent and provided melanoma blood samples to our laboratory.

**References**

1. Bowley TY, Lagutina IV, Francis C, Sivakumar S, Selwyn RG, Taylor E, Guo Y, Fahy BN, Tawfik B, Marchetti D. The RPL/RPS gene signature of melanoma CTCs associates with brain metastasis. Cancer Res Comm. 2022 Nov;2(11):1436-1448.

2. Bowley TY and Marchetti D. Application of CTC discoveries for liquid biopsy: the RPL/RPS gene signature of melanoma CTCs is linked to brain metastasis onset. Clin Exp Metastasis. 2024 Jan 12. https://doi.org/10.1007/s10585-023-10255-1.

3. Biermann J, Melms CJ, Amin AD, Wang Y, Caprio LA, Karz A, *et al*. Dissecting the treatment-naive ecosystem of human melanoma brain metastasis. Cell 2022;185:2591-2608.

4. Guimaraes JC, Zavolan M. Patterns of ribosomal protein expression specify normal and malignant human cells. Genome Biol. 2016 Nov 24;17(1):236.

5. In GK, Poorman K, Saul M, O'Day S, Farma JM, Olszanski AJ, *et al*. Molecular profiling of melanoma brain metastases compared to primary cutaneous melanoma and to extracranial metastases. Oncotarget 2020;11:3118-3128.

6. Davies MA, Liu P, McIntyre S, Kim KB, Papadopoulos N, Hwu WJ, Hwu P, Bedikian A. Prognostic factors for survival in melanoma patients with brain metastases. Cancer. 2011; 117:1687–1696. 10.1002/cncr.25634.

7. Karz A, Dimitrova M, Kleffman K, Alvarez-Breckenridge C, Atkins MB, Boire A. Melanoma central nervous system metastases: An update to approaches, challenges, and opportunities. Pigment Cell Melanoma Res. 2022 Nov;35(6):554-572. doi: 10.1111/pcmr.13059. Epub 2022 Sep 1.

8. Berghoff AS, Schur S, Füreder LM, Gatterbauer B, Dieckmann K, Widhalm G, *et al*. Descriptive statistical analysis of a real life cohort of 2419 patients with brain metastases of solid cancers. ESMO Open 2016;16:1.

9. Schouten, LJ, Rutten, J, Huveneers, HA, Twijnstra, A. (2002). Incidence of brain metastases in a cohort of patients with carcinoma of the breast, colon, kidney, and lung and melanoma. Cancer, 94(10), 2698-2705.

10. Luke JJ, Flaherty KT, Ribas A, Long GV. Targeted agents and immunotherapies: optimizing outcomes in melanoma. Nat Rev Clin Oncol. 2017;14:463-482.

11. Sperduto PW, Mesko S, Li J, Cagney D, Aizer A, Lin NU, *et al.* Survival in patients with brain metastases: summary report on the updated diagnosis-specific graded prognostic assessment and definition of the eligibility quotient. J Clin Oncol 2020;38:3773-3784.

12. Bander ED, Yuan M, Carnevale JA, Reiner AS, Panageas KS, Postow MA, Tabar V, Moss NS. Melanoma brain metastasis presentation, treatment, and outcomes in the age of targeted and immunotherapies. Cancer. 2021 Jun 15;127(12):2062-2073.

13. Wron'Ski M, Arbit E, Burt M, Galicich JH. Survival after surgical treatment of brain metastases from lung cancer: a follow-up study of 231 patients treated between 1976 and 1991. J Neurosurg 1995;83:605-616.

14. Talmadge JE, Fidler IJ. AACR Centennial Series: The biology of cancer metastasis: historical perspective. Cancer Res. 2010 Jul 15;70(14):5649-5669.

15. Dianat-Moghadam H, Azizi M, Eslami-S Z, Cortés-Hernández LE, Heidarifard M, Nouri M, *et al*. The role of circulating tumor cells in the metastatic cascade: biology, technical challenges, and clinical relevance. Cancers. 2020;12:867.

16. Gupta GP, Massague J. Cancer Metastasis: Building a Framework. Cell 2006;127:679-695.

17. Ignatiadis M, Sledge GW, Jeffrey SS. Liquid biopsy enters the clinic — implementation issues and future challenges. Nat Rev Clin Onc. 2021;18:297-312.

18. Werner-Klein M, Scheitler S, Hoffmann M, Hodak I, Dietz K, Lehnert P, Naimer V, Polzer B, Treitschke S, Werno C, Markiewicz A, Weidele K, Czyz Z, Hohenleutner U, Hafner C, Haferkamp S, Berneburg M, Rümmele P, Ulmer A, Klein CA. Genetic alterations driving metastatic colony formation are acquired outside of the primary tumour in melanoma. Nat Comm. 2018 Feb 9;9(1):595.

19. Vishnoi M, Boral D, Liu H, Sprouse ML, Yin W, Goswami-Sewell D *et al*. Targeting USP7 Identifies a Metastasis-Competent State within Bone Marrow–Resident Melanoma CTCs. Cancer Res. 2018;78:5349–5362.

20. Massagué J, Ganesh K. Metastasis-Initiating Cells and Ecosystems. Cancer Discovery. 2021 Apr;11(4):971-994. doi: 10.1158/2159-8290.CD-21-0010.

21. Lambert AW, Pattabiraman DR, Weinberg RA. Emerging Biological Principles of Metastasis. Cell. 2017 Feb 9;168(4):670-691.

22. Joosse SA, Gorges TM, Pantel K. Biology, detection, and clinical implications of circulating tumor cells. EMBO Mol Med. 2015 Jan;7(1):1-11.

23. Nguyen B, Fong C, Luthra A, Smith SA, DiNatale RG, Nandakumar S, *et al*. Genomic characterization of metastatic patterns from prospective clinical sequencing of 25,000 patients. Cell 2022;185:563-575.

24. Lucci A, Hall CS, Patel SP, Narendran B, Bauldry JB, Royal RE, Karhade M, Upshaw JR, Wargo JA, Glitza IC, Wong MKK, Amaria RN, Tawbi HA, Diab A, Davies MA, Gershenwald JE, Lee JE, Hwu P, Ross MI. Circulating Tumor Cells and Early Relapse in Node-positive Melanoma. Clin Cancer Res. 2020 Apr 15;26(8):1886-1895.

25. Aceto N. Bring along your friends: Homotypic and heterotypic circulating tumor cell clustering to accelerate metastasis. Biomedical Journal, 2020: 43:18-23.

26. Sprouse ML, Welte T, Boral D, Liu HN, Yin W, Vishnoi M, Goswami-Sewell D, Li L, Pei G, Jia P, Glitza-Oliva IC, Marchetti D. PMN-MDSCs Enhance CTC Metastatic Properties through Reciprocal Interactions via ROS/Notch/Nodal Signaling. Int J Mol Sci. 2019 Apr 18;20(8):1916.

27. Aceto N, Bardia A, Miyamoto DT, Donaldson MC, Wittner BS, Spencer JA, Yu M, Pely A, Engstrom A, Zhu H, Brannigan BW, Kapur R, Stott SL, Shioda T, Ramaswamy S, Ting DT, Lin CP, Toner M, Haber DA, Maheswaran S. Circulating tumor cell clusters are oligoclonal precursors of breast cancer metastasis. Cell. 2014 Aug 28;158(5):1110-1122.

28. Boral D, Vishnoi M, Liu HN, Yin W, Sprouse ML, Scamardo A *et al.* Molecular characterization of breast cancer CTCs associated with brain metastasis. Nat Comm. 2017 Aug 4;8(1):196.

29. Hurt E, Cheng J, Baβler J, Iwasa J, Beckmann R. SnapShot: Eukaryotic ribosome biogenesis I. Cell. 2023 May 11;186(10):2282-2282.e1.

30. Nerurkar P, Altvater M, Gerhardy S, Schütz S, Fischer U, Weirich C, Panse VG. Eukaryotic Ribosome Assembly and Nuclear Export. Int Rev Cell Mol Biol. 2015;319:107-140.

31. Bowley TY, Merkley SD, Lagutina IV, Ortiz MC, Lee M, Tawfik B, Marchetti D. Targeting Translation and the Cell Cycle Inversely Affects CTC Metabolism but Not Metastasis. Cancers. 2023 Nov 2;15(21):5263.

32. Ebright RY, Lee S, Wittner BS, Niederhoffer KL, Nicholson BT, Bardia A, *et al.* Deregulation of ribosomal protein expression and translation promotes breast cancer metastasis. Science. 2020;367:1468-1473.

33. Micalizzi DS, Ebright RY, Haber DA, Maheswaran S. Translational regulation of cancer metastasis. Cancer Res. 2021;81:517-524.

34. Cao S, Wang JR, Ji S, Yang P, Dai Y, Guo S. Estimation of tumor cell total mRNA expression in 15 cancer types predicts disease progression. Nat Biotechnol. 2022 Nov;40(11):1624-1633.

35. Szczerba BM, Castro-Giner F, Vetter M, Krol I, Gkountela S, Landin J. Neutrophils escort circulating tumour cells to enable cell cycle progression. Nature. 2019 Feb;566(7745):553-557.

36. Ramos MJ, Lui AJ, Hollern DP. The evolving landscape of B cells in cancer metastasis. Cancer Res. 2023 Dec 1;83(23):3835-3845.

37. Willsmore ZN, Harris RJ, Crescioli S, Hussein K, Kakkassery H, Thapa D. B Cells in Patients With Melanoma: Implications for Treatment With Checkpoint Inhibitor Antibodies. Front Immunol. 2021 Jan 25;11:622442.

38. Steinkamp MP, Lagutina I, Brayer KJ, Schultz F, Burke D, Pankratz VS, Adams SF, Hudson LG, Ness SA, Wandinger-Ness A. Humanized Patient-derived Xenograft Models of Disseminated Ovarian Cancer Recapitulate Key Aspects of the Tumor

Immune Environment within the Peritoneal Cavity. Cancer Res Comm. 2023 Feb 22;3(2):309-324.

39. McIntosh BE, Brown ME, Duffin BM, Maufort JP, Vereide DT, Slukvin II. Nonirradiated NOD,B6.SCID Il2rγ-/- Kit(W41/W41) (NBSGW) mice support multilineage engraftment of human hematopoietic cells. Stem Cell Reports. 2015 Feb 10;4(2):171-180.

40. Ordidge RJ, Gibbs P, Chapman B, Stehling MK, Mansfield P. High-speed multislice T1-mapping using inversion-recovery echo-planar imaging. Magn Reson Med 1990;16:238-245.

41. Song Y, Rongvaux A, Taylor A, Jiang T, Tebaldi T, Balasubramanian K, Bagale A, Terzi YK, Gbyli R, Wang X, Fu X, Gao Y, Zhao J, Podoltsev N, Xu M, Neparidze N, Wong E, Torres R, Bruscia EM, Kluger Y, Manz MG, Flavell RA, Halene S. A highly efficient and faithful MDS patient-derived xenotransplantation model for pre-clinical studies. Nat Comm. 2019 Jan 21;10(1):366.

42. Pauken CM, Kenney SR, Brayer KJ, Guo Y, Brown-Glaberman UA, Marchetti D. Heterogeneity of Circulating Tumor Cell Neoplastic Subpopulations Outlined by Single-Cell Transcriptomics. Cancers. 2021 Sep 29;13(19):4885.

43. Alexa A, Rahnenfuhrer JR. topGo: Enrichment analysis for gene ontology. R Package Version 2.42.0; Bioconductor. Buffalo, NY, USA, 2020.

44. Yan F, Jiang L, Ye F, Ping J, Bowley TY, Ness SA. Deep neural network based tissue deconvolution of circulating tumor cell RNA. J Transl Med. 2023 Nov 4;21(1):783.

45. Croft D, O'Kelly G, Wu G, Haw R, Gillespie M, Matthews L, Caudy M, Garapati P, Gopinath G, Jassal B, Jupe S, Kalatskaya I, Mahajan S, May B, Ndegwa N, Schmidt E, Shamovsky V, Yung C, Birney E, Hermjakob H, D'Eustachio P, Stein L. Reactome: a database of reactions, pathways and biological processes. Nucleic Acids Res. 2011 Jan;39(Database issue):D691-7.

46. Hao Y, Stuart T, Kowalski MH, Choudhary S, Hoffman P, Hartman A. Dictionary learning for integrative, multimodal and scalable single-cell analysis. Nat Biotech. 2024 Feb;42(2):293-304.

47. Hao Y, Hao S, Andersen-Nissen E, Mauck WM 3rd, Zheng S, Butler A. Integrated analysis of multimodal single-cell data. Cell. 2021 Jun 24;184(13):3573-3587.e29.

48. Noffsinger B, Witter A, Sheybani N, Xiao A, Manigat L, Zhong Q, Taori S, Harris T, Bullock T, Price R, Purow B. Technical choices significantly alter the adaptive immune response against immunocompetent murine gliomas in a model-dependent manner. J Neurooncol. 2021 Sep;154(2):145-157.

49. Eroglu Z, Holmen SL, Chen Q, Khushalani NI, Amaravadi R, Thomas R, Ahmed KA, Tawbi H, Chandra S, Markowitz J, Smalley I, Liu JKC, Chen YA, Najjar YG, Karreth FA, Abate-Daga D, Glitza IC, Sosman JA, Sondak VK, Bosenberg M, Herlyn M, Atkins MB, Kluger H, Margolin K, Forsyth PA, Davies MA, Smalley KSM. Melanoma central nervous system metastases: An update to approaches, challenges, and opportunities. Pigment Cell Melanoma Res. 2019 May;32(3):458-469.

50. Elhamamsy AR, Metge BJ, Alsheikh HA, Shevde LA, Samant RS. Ribosome biogenesis: a central player in cancer metastasis and therapeutic resistance. Cancer Res. 2022;8213:2344-2353.

51. Alix-Panabières C, Pantel K. Challenges in circulating tumour cell research. Nat Rev Cancer. 2014 Sep;14(9):623-631.

52. Cox TR, Gartland A, Erler JT. The pre-metastatic niche: is metastasis random? Bonekey Rep. 2012 May 2;1:80.

53. Seyfried TN, Huysentruyt LC. On the origin of cancer metastasis. Crit Rev Onc. 2013;18(1-2):43-73.

54. Damsky WE, Theodosakis N, Bosenberg M. Melanoma metastasis: new concepts and evolving paradigms. Oncogene. 2014 May 8;33(19):2413-2422.

55. Obrador E, Salvador R, López-Blanch R, Jihad-Jebbar A, Alcácer J, Benlloch M, Pellicer JA, Estrela JM. Melanoma in the liver: Oxidative stress and the mechanisms of metastatic cell survival. Semin Cancer Biol. 2021 Jun;71:109-121.

56. Vishnoi M, Liu NH, Yin W, Boral D, Scamardo A, Hong D. The identification of a TNBC liver metastasis gene signature by sequential CTC-xenograft modeling. Mol Onc. 2019 Sep;13(9):1913-1926.

57. Li D, Wang J. Ribosome heterogeneity in stem cells and development. J Cell Biol. 2020;219:e202001108.

58. Loveland AB, Koh CS, Ganesan R, Jacobson A, Korostelev AA. Structural mechanism of angiogenin activation by the ribosome. Nature. 2024 Jun 20;630:769-776.

59. Yang Y, Chen X, Pan J, Ning H, Zhang Y, Bo Y, Ren X, Li J, Qin S, Wang D, Chen M, Zhang Z. Pan-cancer single-cell dissection reveals phenotypically distinct B cell subtypes. Cell. 2024 Aug 22;187:4790-4811.

60. Ma J, Wu Y, Ma L, Yang X, Zhang T, Song G. A blueprint for tumor-infiltrating B cells across human cancers. Science. 2024 May 3;384(6695):eadj4857.

61. Biswas S, Mandal G, Payne KK, Anadon CM, Gatenbee CD, Chaurio RA. IgA transcytosis and antigen recognition govern ovarian cancer immunity. Nature. 2021 Mar;591(7850):464-470.

62. Zhong Z, Nan K, Weng M, Yue Y, Zhou W, Wang Z. Pro- and Anti- Effects of Immunoglobulin A- Producing B Cell in Tumors and Its Triggers. Front Immunology. 2021 Nov 19;12:765044.

63. Tan R, Nie M, Long W. The role of B cells in cancer development. Front. Oncology. 2022 Aug 11;12:958756.

64. Ou Z, Wang Y, Liu L, Li L, Yeh S, Qi L, Chang C. Tumor microenvironment B cells increase bladder cancer metastasis via modulation of the IL-8/androgen receptor (AR)/MMPs signals. Oncotarget. 2015 Sep 22;6(28):26065-26078.

65. Bindea G, Mlecnik B, Angell HK, Galon J. The immune landscape of human tumors: Implications for cancer immunotherapy. Oncoimmunology. 2014 Jan 1;3(1):e27456.

66. Teng MW, Galon J, Fridman WH, Smyth MJ. From mice to humans: developments in cancer immunoediting. J Clin Invest. 2015 Sep;125(9):3338-3346.

67. Yuen GJ, Demissie E, Pillai S. B lymphocytes and cancer: a love-hate relationship. Trends Cancer. 2016 Dec;2(12):747-757.

68. Cimino-Mathews A, Ye X, Meeker A, Argani P, Emens LA. Metastatic triple-negative breast cancers at first relapse have fewer tumor-infiltrating lymphocytes than their matched primary breast tumors: a pilot study. Hum Pathology. 2013 Mar; 44:2055-2063.

## Figure Legends

**Figure 1.**

Metastatic patterns of first generation CDX mice by IVIS imaging. Gender-specific HuNBSGW (**A**) and immunodeficient NBSGW (**B**) mice were engrafted by intracardiac injection with CTC-derived clonal cells (70W-SM3-Luc2; 5.0x10E5/animal). IVIS imaging was performed every week to evaluate metastatic onset. The last IVIS time point (5 weeks) is shown. Mice with MBM are circled. Following necropsy, pathologic evaluation revealed multi-focal MBM in HuNBSGW (**C**) and NBSGW (**D**) groups. MBM (N=5 per group) were selected for tumor cell dissociation, isolation, and reinjection to obtain the second generation CDXs. **E**, Representative MBM-generated liver metastasis in second-generation HuNBSGW CDX mice. See “Materials and Methods” for experimental details.

**Figure 2.**

The melanoma brain-liver metastasis axis. **A-B**, MBM-generated liver metastasis and MBM of second-generation mice. MBM/liver mets (yellow arrows) from second-generation HuNBSGW (**A**) and NBSGW (**B**) mice engrafted via intracardiac injection with first-generation CDX MBM cells (5.0x10E5 cells/animal). Quantification of liver metastasis shows higher %, number and size of liver mets in HuNBSGW mice (bottom

panel). **C**, Statistical significance (***$p$-value < 0.001) for presence of brain (MBM) and liver metastasis, showing distinct onset in the second generation CDXs, injected with blood vs MBM-dissociated cells from first-generation CDXs. See “Materials and Methods” for experimental details.

**Figure 3.**

Commonality and upregulation of the MBM RPL/RPS CTC gene signature in the second generation HuNBSGW CDXs. **A**, RNA-Seq gene expression profiling showing distinct clustering patterns between cells of liver (green) and brain (red) metastasis (left panel). Upregulation of the CTC RPL/RPS gene signature in MBM-generated liver mets vs MBM is shown in the right panel, calculated in counts per million. Mean values of the 21 RPL/RPS members of the CTC signature are indicated (red). **B**, Statistically significant RNA-Seq pathways generated by Reactome database analyses. Pathways highlighted in yellow are the same of RPL/RPS CTC gene expression pathways (1). See “Materials and Methods” for experimental details.

**Figure 4.**

Capture and interrogation of CTCs from HuNBSGW and NBSGW CDXs by FDA-approved CTC Parsortix platform. Blood of the second-generation CDXs was collected at the end of the study and immunostained for visualization of single CTCs (MelA+/DAPI+/CD45- cells) (**A**), and CTC clusters (**B**). **C**, Cells from healthy donors blood (MelA-/DAPI+/CD45+) were stained in parallel as control. Bottom panel shows model-specific, gender-specific number of single CTCs and CTC clusters (2-cell or greater) quantified by high-definition confocal microscopy in second-generation CDXs. A significant increase of CTCs/CTC clusters were detected in HuNBSGW CDXs, regardless of gender (red box). See “Materials and Methods” for experimental details.

**Figure 5.**

RNA-Seq analyses of blood and brain from second-generation HuNBSGW and NBSGW mice. **A-B**, CTCs from blood of second-generation HuNBSGW CDXs (N=3) were harvested via Parsortix, followed by RNA-Seq interrogation. Distinct unsupervised

hierarchical clustering of gene expression between HuNBSGW CTCs and uninjected CTC-derived clonal cells (**A**), or blood-derived CTCs from immunodeficient NSG mice (**B**). **C**, RNA-Seq analyses of cells isolated from MBM cells of second-generation HuNBSGW/NBSGW CDXs with heat maps showing differential clustering of MBM-derived cells in the presence or absence of human immune cells. **(Bottom panels)**, Top molecular pathways resulting from comparisons in HuNBSGW vs NBSGW CDXs (Reactome pathway database). All RNA-Seq analyses showed the presence of B-cell related pathways in HuNBSGW CDXs (highlighted in yellow). See "Materials and Methods" for experimental details.

**Figure 6.**

Detection and quantitation of CTC (MelA+/DAPI+/CD45-):B cell (CD19+/DAPI+/CD45+) clusters in melanoma patients blood by Parsortix. Visualization of CTC:B cell clusters in primary (**A**), metastatic (**B**) melanoma patients, and single B cells (**C**) in patient samples (CD19+/DAPI+/MelA- cells) was performed using high-definition Zeiss 800 confocal microscopy (left panels). Right panel shows number of CTC:B cell clusters/ patient sample analyzed. High numbers of heterotypic CTC:B cell clusters were detected in blood of primary melanoma patients (red box). Patients' clinical parameters are shown in Supplementary Table 4. See "Materials and Methods" for experimental details.

**Figure 7.**

Spatial single-cell gene expression analysis of CTC-derived cells:B cell interactions employing 10x Genomics Xenium platform (www.10xgenomics.com). HuNBSGW A2.1 mice were engrafted via intracardiac injection with CTC-derived clonal cells (70W-SM3-Luc2; 5.0x $10^5$ cells/animal). **A**, Dim Plot shows 2D scatter plot representing cell clusters in reduced space. Cell annotations are shown on the right. Brain (**B,** top left panel) and liver (**B,** top right panel) metastases of second-generation CDXs were isolated, paraffin-embedded, sectioned, and analyzed via the 10x Xenium platform. An image of the whole tissue section is presented (left panel), followed by two close-up images (right panels). CTC-derived melanoma cells were identified as S100A1+ cells (red), while B cells were defined as BCR+ cells (green). Only melanoma cells showed extensive

RPL23+ and RPL35A+ gene expression as significant members of the RPL/RPS CTC signature (31). Bottom panel shows quantitation of percentage and number of S100+ and BCR+ cells/mm$^2$**.** See “Materials and Methods” for experimental details.

**Figure 8.**

Spatial single-cell protein expression analyses of HuNBSGW tumor tissues by HALO™ platform (Indica Lab). HuNBSGW A2.1 tumor tissues: **A**, humanized brain, **B**, humanized liver were cut on Microtome right after the Xenium sections and stained for MelA and CD19 to visualize melanoma and B cells, respectively (top panel). Positive cells were quantified using HALO software. Bottom panel shows numbers and percentages of MelA+ and CD19+ cells in the whole section. See “Materials and Methods” for experimental details.

# Figure 1

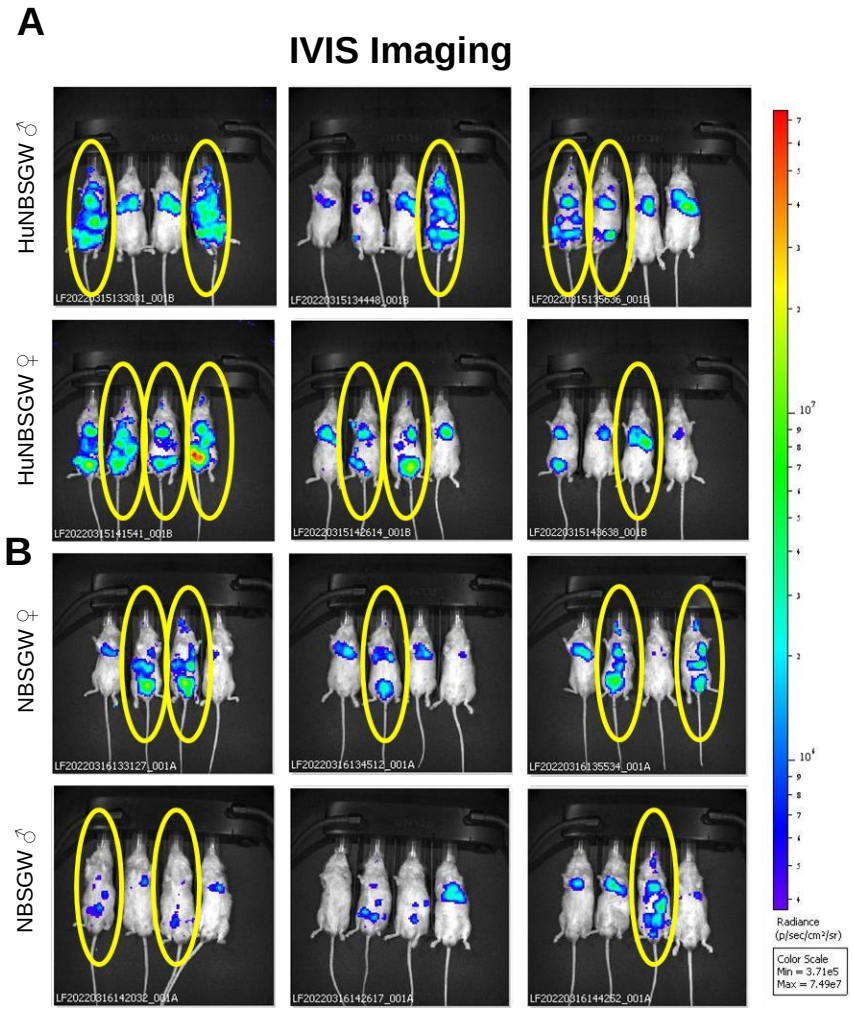


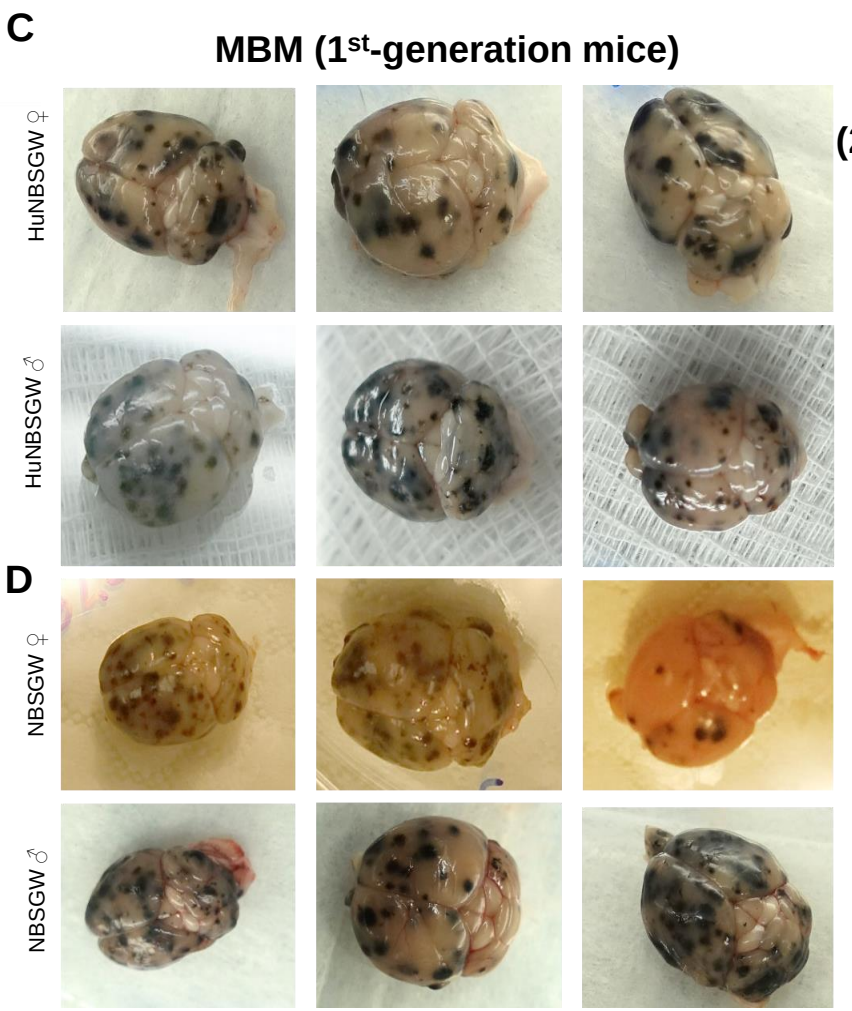


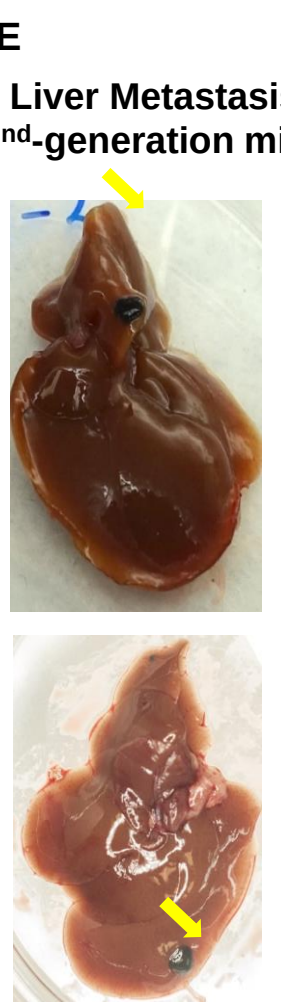

# Figure 2

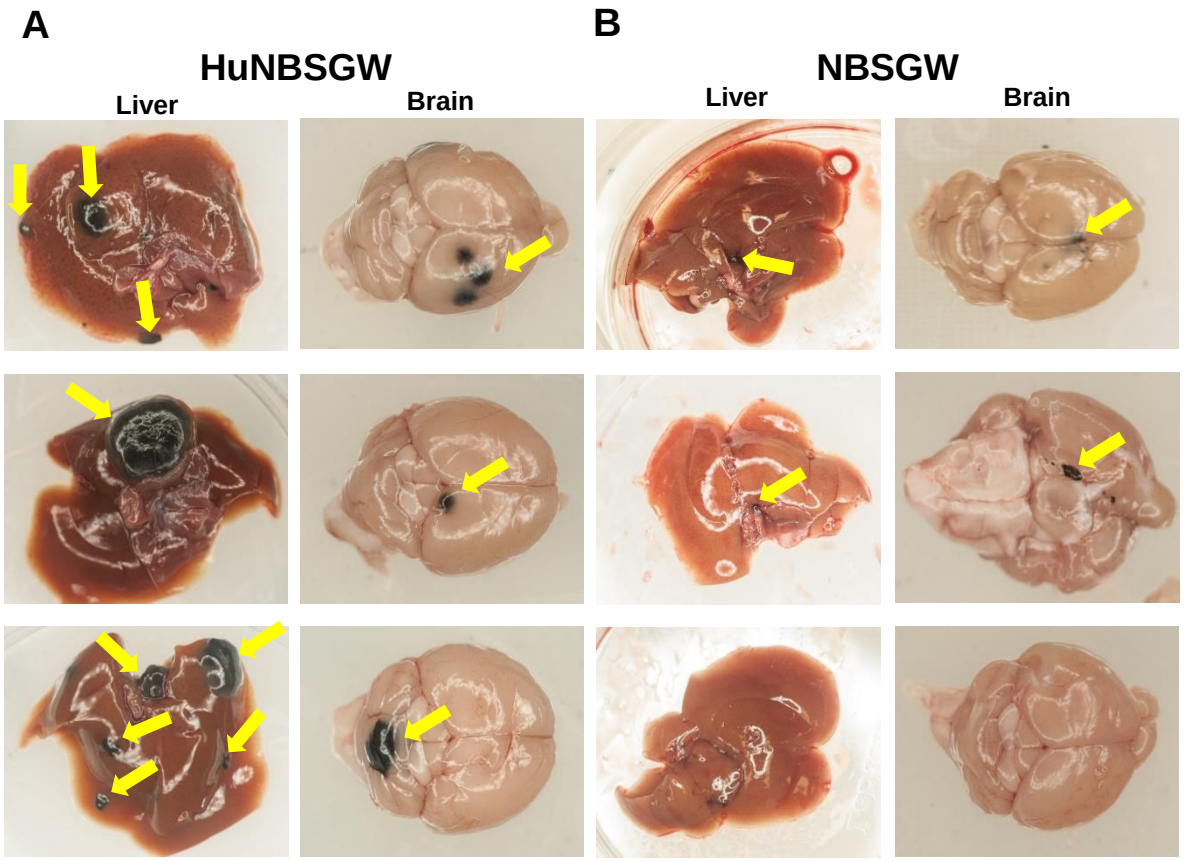


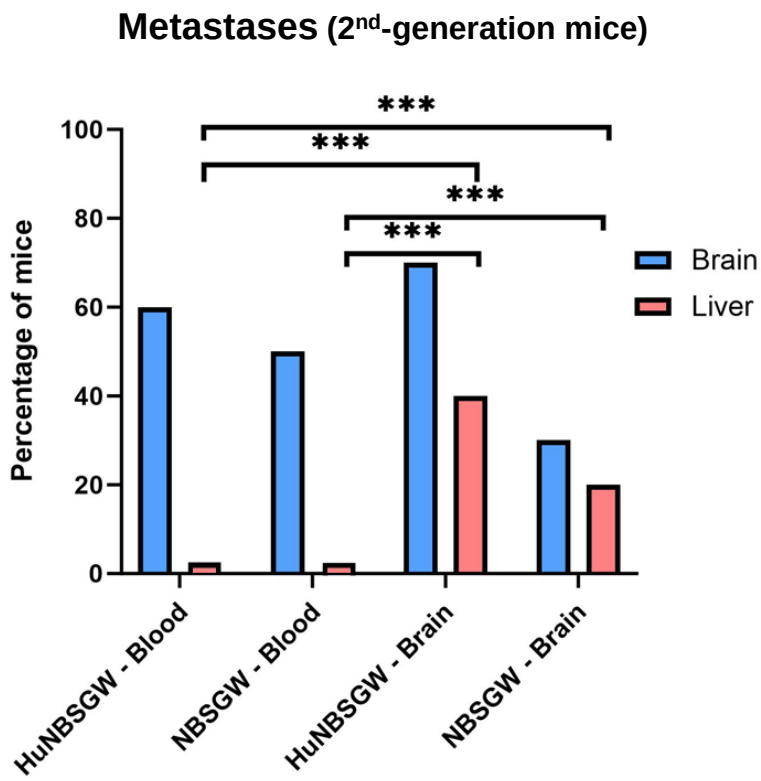


## Quantification of liver metastasis

| Tissue type | % mice with liver mets | Number of mets/liver | Liver mets volume ($mm^3$) |
|---|---|---|---|
| HuNBSGW liver | 40% | 5 | 83 |
| NBSGW liver | 20% | 1 | 6 |

# Figure 3

**Upregulation of the RPL/RPS CTC signature in MBM-generated liver mets**

| | MBM | Liver |
|---|---|---|
| RPL12 | 161.8 | 569.0 |
| RPL13 | 635.0 | 2439.9 |
| RPL18A | 22.1 | 1021.7 |
| RPL19 | 753.5 | 758.5 |
| RPL23 | 158.7 | 404.5 |
| RPL26 | 318.8 | 1040.6 |
| RPL35A | 303.1 | 1207.0 |
| RPL37 | 179.7 | 410.8 |
| RPL38 | 204.3 | 739.7 |
| RPL6 | 77.8 | 483.6 |
| RPL7 | 404.2 | 1262.3 |
| RPL7A | 377.3 | 2155.1 |
| RPS12 | 118.7 | 966.7 |
| RPS15A | 77.0 | 1048.4 |
| RPS18 | 86.2 | 2521.7 |
| RPS24 | 225.0 | 306.9 |
| RPS26 | 120.1 | 423.3 |
| RPS28 | 16.8 | 246.6 |
| RPS5 | 133.5 | 3005.5 |
| RPS7 | 59.9 | 624.3 |
| RPSA | 71.4 | 434.1 |
| **MEAN** | **214.5** | **1051.0** |

**A**

**RNA-Seq**

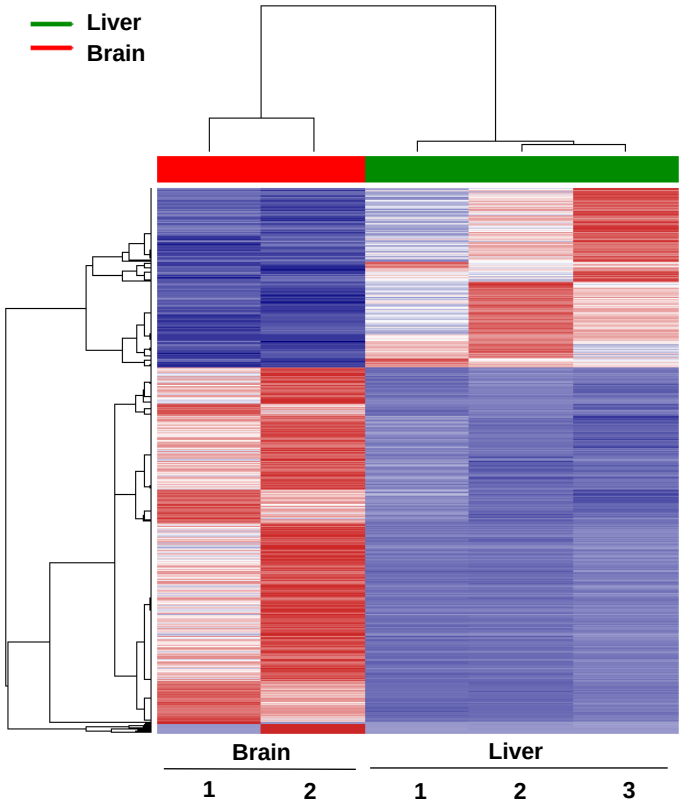


**B**

**RNA-Seq pathways**

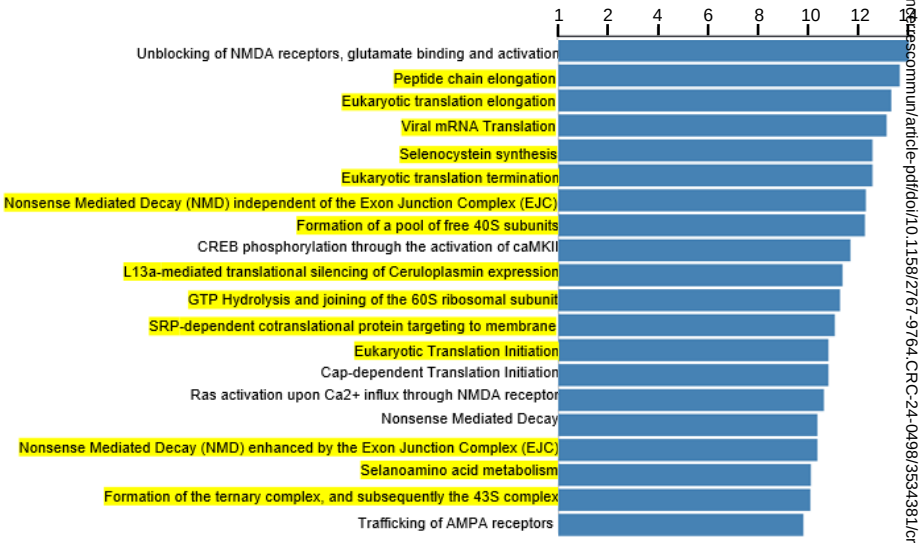


**Enrichment Ratio**

# Figure 4

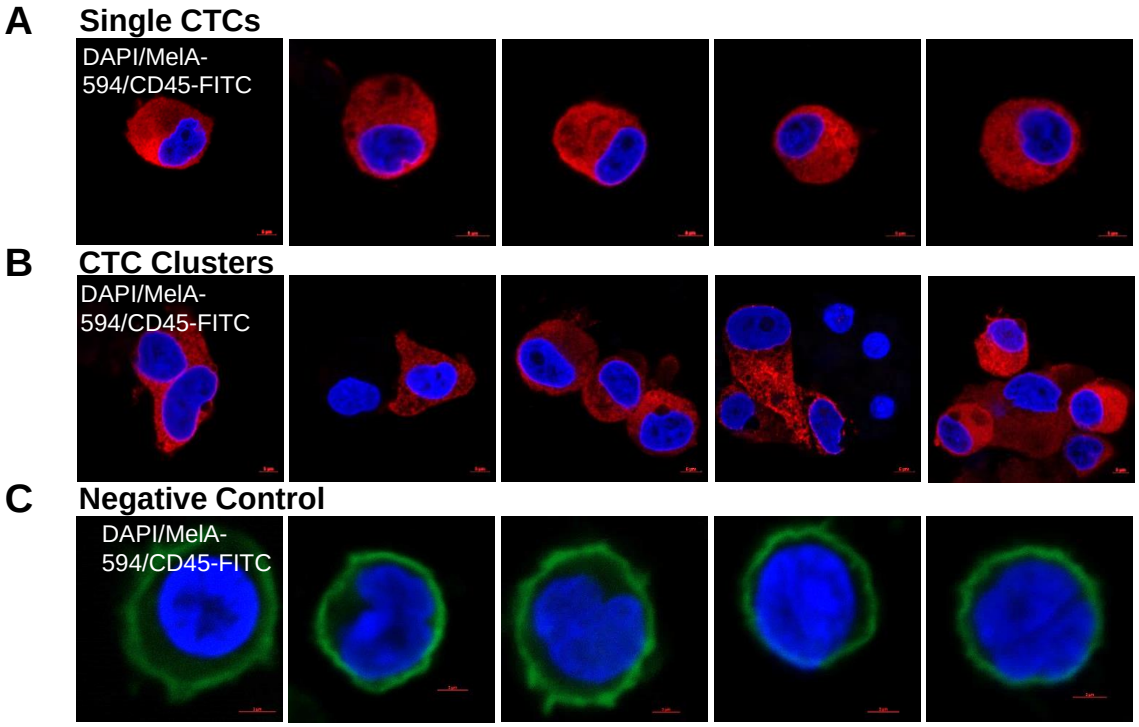


## CTC/CTC clusters enumeration by Parsortix™

| | NBSGW males | NBSGW females | HuNBSGW males | HuNBSGW females |
|---|---|---|---|---|
| | CTCs/mL | | | |
| Single cells | 41 | 10 | 183 | 190 |
| 2-cell | 32 | 10 | 121 | 161 |
| 3-cell | 21 | 11 | 33 | 92 |
| 4-cell | 5 | 0 | 21 | 61 |
| 5-cell or greater | 0 | 0 | 18 | 22 |

# Figure 5

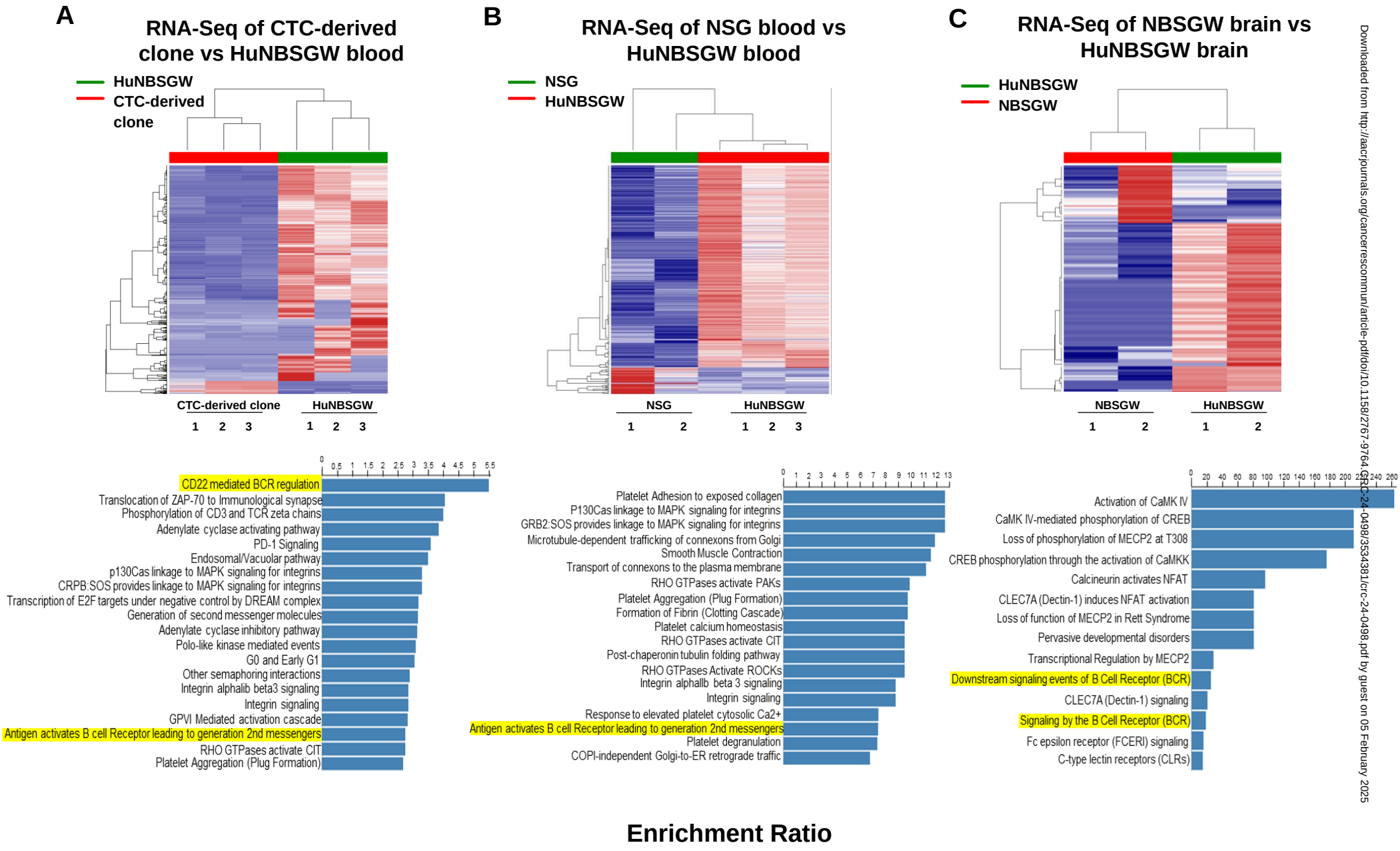

# Figure 6

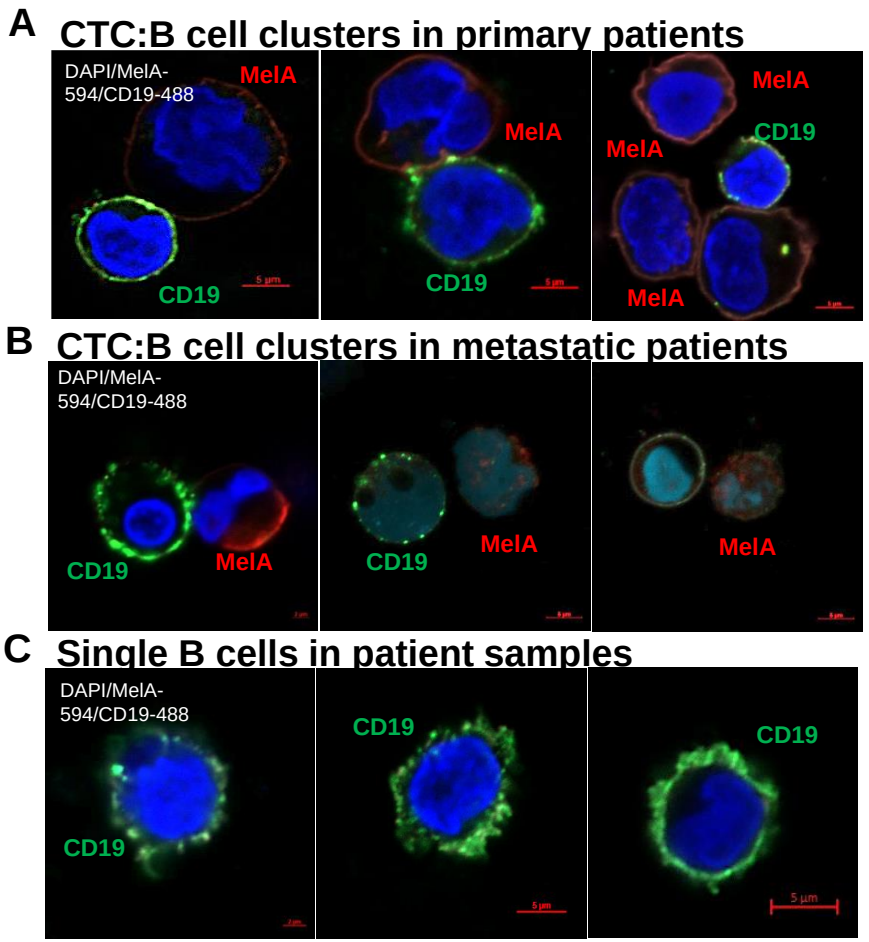


## CTC:B cell clusters are elevated in primary vs. metastatic melanoma patients

| Patient ID | Metastasis | Treatment | CTC:B cell clusters/10mL |
|---|---|---|---|
| Primary patient 1 | None | None | 43 |
| Primary patient 2 | None | None | 19 |
| Primary patient 3 | None | None | 18 |
| Primary patient 4 | None | None | 33 |
| Metastatic patient 1 | Thigh | Nivolumab | 2 |
| Metastatic patient 2 | Neck, chest, abdomen, pelvis, muscle, lymph nodes, ribs, lung | Nivolumab Ipilimumab | 1 |
| Metastatic patient 3 | Pulmonary nodules, ribs, spleen, liver | Nivolumab Ipilimumab | 2 |
| Metastatic patient 4 | Breast, avilla, lower extremity | Nivolumab | 2 |

# Figure 7

**A**

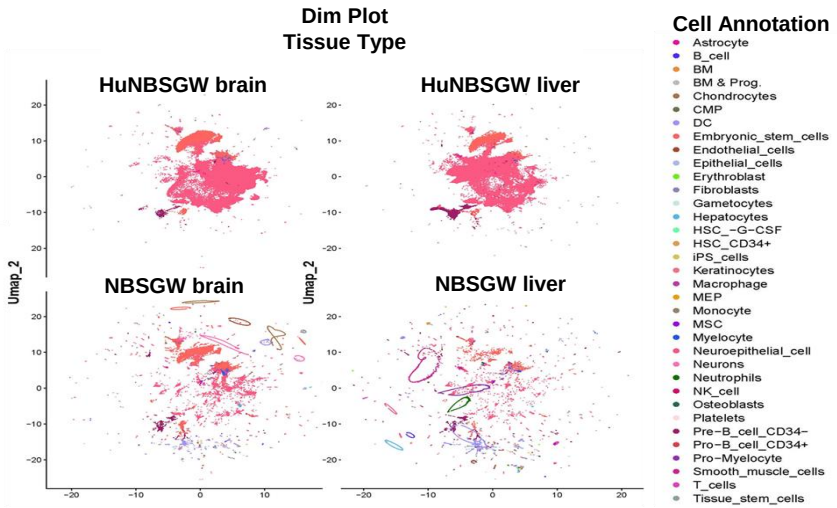


**B** Xenium analyses of HuNBSGW brain

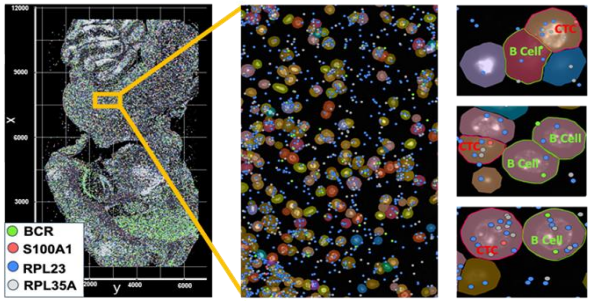


**C** Xenium analyses of HuNBSGW liver

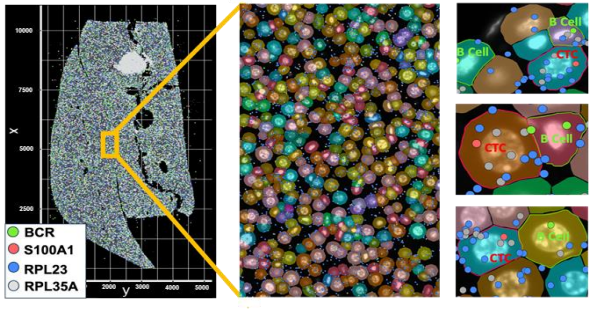


## Quantification of 10x Xenium analyses of HuNBSGW tissues

| Tissue | Total Cells/mm² | S100A1+ Transcripts/mm² | % S100A1+ Transcripts/Cell | BCR+ Transcripts/mm² | % BCR+ Transcripts/Cell |
|---|---|---|---|---|---|
| Liver | 3.24 | 0.06 | 2 | 0.38 | 12 |
| Brain | 2.15 | 0.06 | 3 | 0.95 | 44 |

# Figure 8

**A** **HALO analyses of HuNBSGW brain**

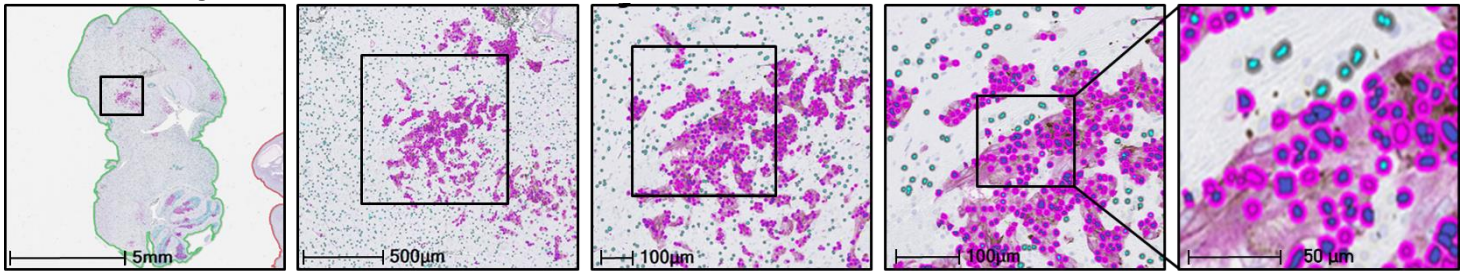


**B** **HALO analyses of HuNBSGW liver**

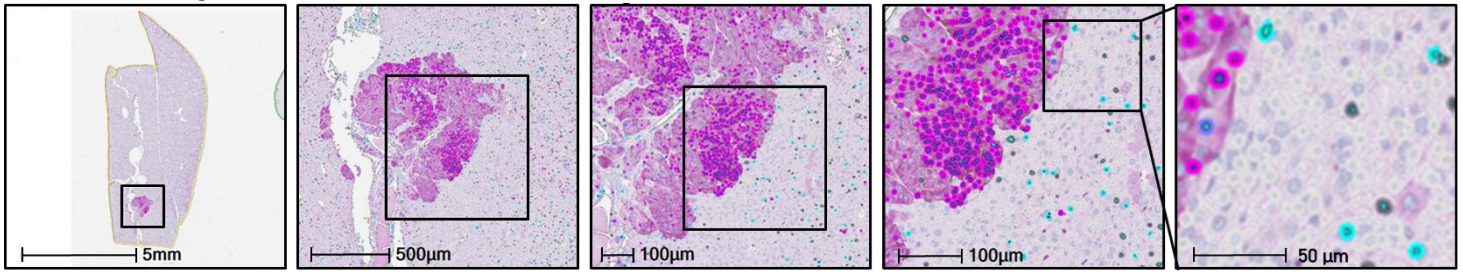


## Quantification of HALO analyses of HuNBSGW tissues

| Tissue | Total Cells/mm² | MelA+ Cells/mm² | % MelA+ Cells | CD19+ Cells/mm² | % CD19+ Cells | SD |
|---|---|---|---|---|---|---|
| Liver | 3.32 | 2.32 | 70.08 | 0.263 | 7.92 | 1.02 |
| Brain | 1.78 | 0.178 | 9.98 | 0.817 | 45.83 | 0.03 |